Neuropsychologia 124 (2019) 226–235

Contents lists available at ScienceDirect

Neuropsychologia

journal homepage: www.elsevier.com/locate/neuropsychologia

A neural substrate of early response capture during conflict tasks in sensory areas

Yael Salzer[a,*], Gilles de Hollander[a], Leendert van Maanen[b], Birte U. Forstmann[a]

[a] Integrative Model-based Cognitive Neuroscience Research Unit, University of Amsterdam, 1018 WS, The Netherlands
[b] Department of Psychological Methods, University of Amsterdam, 1018 WS, The Netherlands

ARTICLE INFO

Keywords:
Cognitive neuroscience
Early response capture
Multivariate pattern analysis
Simon task
Somatosensory

ABSTRACT

Studies that aim to understand the neural correlates of response conflicts commonly probe frontal brain areas associated with controlled inhibition and decision processes. However, untimely fast conflict errors happen even before these top-down processes are engaged. The dual-route model proposes that during conflict tasks, as soon as the stimulus is presented, two early processes are immediately at play. The task-relevant and task-irrelevant processes generate either compatible responses, when all stimulus features align, or incompatible responses, when stimulus features are in conflict. We aimed to find a neural substrate of these two processes by means of relating the quality of the representation of stimulus features in visual and somatosensory brain areas to responses in conflict tasks. Participants were scanned using fMRI while performing somatosensory and visual Simon tasks. The fMRI data were then analysed using a MVPA in early visual and somatosensory cortices. In agreement with our hypotheses, results suggest that the sensory representation of the task-relevant and task-irrelevant features drive erroneous trials. These results demonstrate that traces of response conflicts can arise already in sensory brain areas and that the quality of the representations in these regions can account for an early response capture by irrelevant stimulus features.

1. Introduction

A cognitive conflict is an information mismatch stemming from incompatible or opposing stimulus features. For example, in the Stroop task (Stroop, 1935), a participant is asked to name the ink-colour of a colour-word. Responses slow down, and errors are more common, when the task-relevant ink colour and task-irrelevant word identity are incompatible. Moreover, as was observed in a large variety of conflict tasks, fast incompatible trials are more prone to errors, as compared to slow or compatible trials (Stroop task: Dittrich and Stahl, 2017; Flanker task: Coleman et al., 2017; Simon task: Wylie et al., 2009; masked priming task: Ellinghaus and Miller, 2017). The underlying process that drives these fast errors is regarded as early response capture by irrelevant information (van Maanen et al., 2015). In the Simon task, a classic stimulus-response conflict task, participants are typically asked to identify a figure, and response with a left or right key-press accordingly. The spatial location of the stimulus, displayed left or right of a fixation, is task-irrelevant. Nevertheless, participants respond faster and more accurately when the appropriate key spatially matches the stimulated side (i.e., congruent condition) than when it does not (i.e., incongruent condition). The activation of the response system by the task irrelevant stimulus location is represented in the plot of accuracy as function of response time (i.e., conditional accuracy function, CAF), by the near-asymptote accuracy of congruent responses, but low accuracy in the fast portion of incongruent responses (Forstmann et al., 2008b; Ridderinkhof, 2002a).

The present study proposes a means to trace the neural correlates of early response capture based on a structural model developed for the studying of stimulus-response conflicts, the *dual-route model* (De Jong et al., 1994; Ridderinkhof, 2002b). In the dual-route model it is assumed that two processes take place in parallel (Fig. 1). One process refers to a task-relevant indirect route that processes the deliberate response decision based on task demands. The other process refers to a task-irrelevant route, where the spatial code directly activates a response that corresponds with the relative location of the stimulus (Kornblum et al., 1990). In the congruent condition, both task-relevant and irrelevant dimensions of the stimulus generate the same response. In the incongruent condition, the irrelevant response contradicts the correct response because the stimulus onset automatically primes the spatially corresponding however incorrect response. The present study aimed to investigate the perceptual aspect of the early response process, to trace the neural correlates of early response capture in sensory brain

* Corresponding author.
E-mail address: salzerit@gmail.com (Y. Salzer).

https://doi.org/10.1016/j.neuropsychologia.2018.12.009
Received 10 June 2018; Received in revised form 29 October 2018; Accepted 11 December 2018
Available online 13 December 2018
0028-3932/

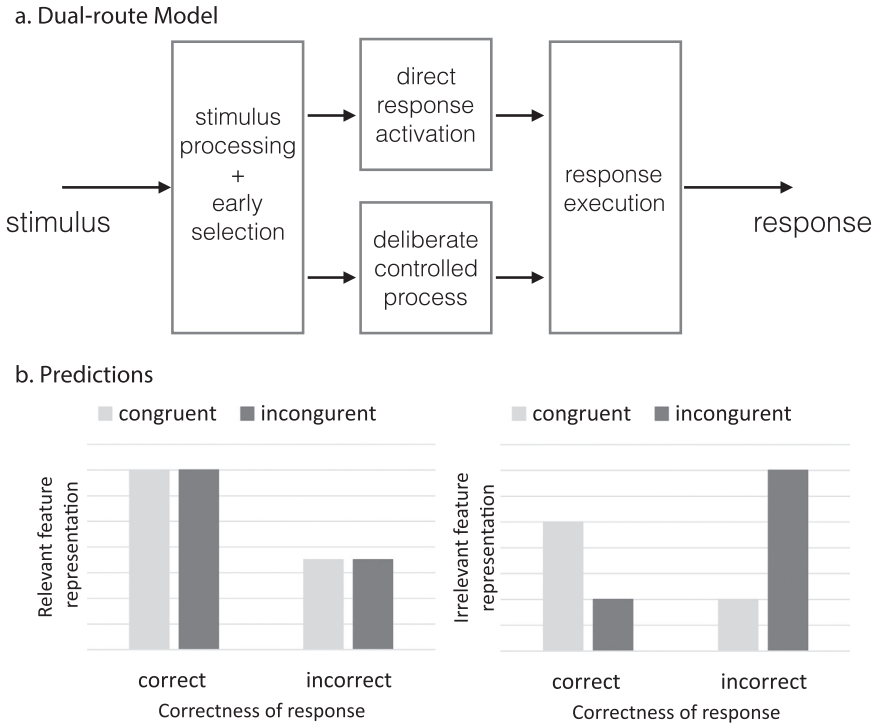

Fig. 1. [a] Dual-route model. [b] Predicted magnitude of relevant and irrelevant feature representation as function of congruency and correctness of response are illustrated in left and right panels, respectively.

areas that code for the relevant and irrelevant stimulus features, which are later expressed as the wrong response.

Within the framework of the dual-route model we propose that the strength of the stimulus' features representations in sensory areas should account for response behaviour. The strength of the relevant and irrelevant stimulus feature representations will drive, at least to some extent, the influence of the relevant and the irrelevant route on the final response (Salzer et al., 2017). If a stimulus feature is more or less sharply encoded, this will offer more or less reliable information to downstream decision-forming areas. By reverse inference, we formulate three concrete predictions (Fig. 1.b). (A) In both congruent and incongruent trials, relevant feature representations will be stronger on correct trials relative to incorrect trials. Secondly, with congruent trials, relevant and irrelevant features align and activate the same response-code, facilitating the correct response. We assume that the infrequent congruent errors are driven by noise that originates from stochastic or external processes that are not explicitly described by the dual-route model. It is likely for noise to drive an error when the aligned relevant and irrelevant features in a congruent trial are represented very noisily, resulting in a lapse. Thus, (B) the strength of the irrelevant feature representation should on average be higher during correct congruent trials compared to erroneous congruent trials. Finally, (C) higher activity in the irrelevant route, during incongruent trials, is expected to increase the likelihood of early response capture (Ridderinkhof, 2002b) yielding incorrect responses. Thus, the irrelevant spatial feature representation will be stronger on incorrect incongruent trials, relative to correct incongruent trials.

2. Material and methods

Our predictions were tested in a functional magnetic resonance imaging (fMRI) experiment. To quantify the strength of the stimulus feature representation in the brain, multivariate pattern analysis (MVPA) was used. MVPA is a neuroimaging analysis approach which trains a model of how stimulus features are encoded in the brain using supervised learning. The trained model can then be used to quantify the encoding of stimulus features in previously unseen data on a trial-by-trial basis (Haxby et al., 2014; Kriegeskorte, 2011). We applied MVPA during visual and somatosensory Simon tasks. In a typical visual Simon task, the participant is asked to identify a visual image presented to the left or right of a fixation cross (Forstmann et al., 2008b). In a somatosensory Simon task, the participant is asked to identify a vibrotactile pulsation presented on an area located on the left or right side of the body (Salzer et al., 2014). Typically, the participant is asked to make a decision by pressing a button with the left or right hand. The participant is expected to ignore the spatial location of the stimulus, since it is irrelevant to the task-at-hand. Nevertheless, on trials in which the stimulus is positioned contralateral to the correct response, the participant is usually slower and more likely to make fast errors (Duprez et al., 2016; Houvenaghel et al., 2016; Salzer et al., 2014; Wylie et al., 2009).

In an exploratory first fMRI study, we used a comparable experimental design, however, with some crucial differences in both the visual and tactile domain (please see supplementary materials for design and results). This study and results helped us to gain insights in the effect size of the manipulations. In the second fMRI experiment reported here, we revised the experimental setup in such a way as to allow for a conceptual replication while increasing the effect size.

2.1. Participants

Thirty-three healthy participants were scanned. Data of five participants was not analysed due to technical failure in the scanner or during data transfer. All remaining 28 participants (14 females; 24.9 mean age, std. age 6.9, range 19 – 46) had normal or corrected to normal vision and no history of neurological or psychological disorders. The study was approved by the local ethical committee of the University of Amsterdam, The Netherlands. All participants gave written informed consent and received monetary reward for their participation.

2.2. Experimental design and statistical analysis

2.2.1. Procedure

The participants first performed a practice session of 16 visual Simon trials and 16 somatosensory Simon trials in a preparation room, after which they were screened for MRI. While scanning, they performed 208 trials of a visual Simon task, and 208 trials of a somatosensory Simon task, divided over 8 runs consisting of 52 trials each. Each run lasted 5:08 min. The order of modality was counterbalanced across participants. Trial length varied between 4, 4.5, 5, 5.5, 6, 6.5, 7, 7.5 and 8 s. A trial started with a black fixation cross for 300 ms, followed by a second red fixation cross for another 300 ms. After the second fixation cross, the target stimulus was presented for 450 ms. To probe for errors in both congruent and incongruent conditions, participants were encouraged to respond as fast as possible. If a response was not recorded within 500 ms (visual) or 750 ms (somatosensory) from onset of the stimulus, a "too slow" message appeared on screen for 1500 ms. At the end of each trial, a black cross was presented during the remainder of the fixed trial time. The participant was instructed to fixate at the cross, however their gaze was not monitored.

The somatosensory target stimulus, generated by piezoelectric vibratory stimulator (custom made by Mag Design and Engineering, Redwood City, CA, USA), was a 250-Hz vibration of either a single continuous 450 ms pulse (i.e., continuous stimulus) or a fast sequence of three equally spaced 75 ms pulses with a total duration of 450 ms (i.e., intermittent stimulus). Two piezoelectric vibrotactors were attached to the back of the left and right hands. An equal number of intermittent and continuous stimuli were introduced in each run, activated by either right or left vibrotactor (Fig. 2). The visual target stimulus was a black-and-white image of a house or a face. An equal number of houses and faces were introduced in each run, to the left or right of the fixation cross. Participant's hands rested on left and right response boxes, index fingers placed on the response keys. The mapping of (continuous/intermittent, house/face) to response key (left/right) was fully counterbalance across participants. The instructions were displayed on screen before each run.

2.2.2. MRI scanning protocol

The experiment was carried out on a Philips 3.0T Achieva whole-body MRI scanner (The Netherlands). A T2*-weighted EPI sequence was used to measure the BOLD signal, with a 32-channel head coil. The order of imaging acquisition was ascending, covering the whole brain of participants. For each functional volume, 43 slices were collected resulting in a 2.5 mm isotropic resolution over a 96 × 94 voxel matrix (TR = 2500.001 ms, TE = 27.6 ms, and FA = 77.2°). Prior to the functional runs, a 3-D, high-resolution, T1-weighted whole-brain image was acquired (1 × 1 × 1 mm^3, TR = 8.506, TE = 3.93 FA = 8°). To correct for field inhomogeneity, a corresponding B0 field map scan of 128 slices was also acquired (3 × 3 × 3 mm^3, TR = 10.964 ms, TE echo = 3.07 ms, delta TE = 5 ms, FA = 8°). Visual stimuli were presented to the participants on a back-projection screen, which could be viewed via a mirror system attached to the MRI head coil. Somatosensory piezoelectric actuators were attached by adjustable Velcro strips to the back of the participant's hands.

2.2.3. Pre-processing

The data were corrected for inhomogeneity in the main magnetic field (B0), using the acquired B0 field map and the FUGUE procedure as implemented in FSL (Jenkinson, 2004; Jezzard and Balaban, 1995). The data was processed using the standard FSL FEAT pre-processing pipeline (Smith et al., 2004; Woolrich et al., 2009), as implemented in the NiPype fMRI pipeline framework (Gorgolewski et al., 2011). This pipeline motion-corrects the data using the MCFLIRT algorithm, and smooths the data at full-width-half-maximum (FWHM) of 5 mm using the SUSAN algorithm. Brain Extraction Tool (FSL BET) was used on individual anatomical scans (Smith, 2002). All functional datasets were individually registered to the individual participant high-resolution anatomical images using FSL FLIRT.

2.2.4. Univariate analysis

Two general linear models were fitted to the MRI data in a massively univariate fashion (Worsley and Friston, 1995). In the first model, congruency (congruent, incongruent) and task-irrelevant feature, the stimulus side (left, right), as well as outlier motion parameters, and were used as predictors. In the second model, congruency (congruent, incongruent) and task-relevant feature (visual: house, face; somatosensory: intermittent, continuous), as well as outlier motion parameters were used as predictors. Contrast maps were generated for each participant. Next, to perform group analysis, the individual contrast maps were normalized toward MNI space by linear and subsequent non-linear transformation using ANTS. Higher-level analyses were carried out using FSL's FLAME. For the whole-brain analysis we only report regions with a voxel-wise threshold of $z > 3.1$ and a cluster-wise threshold of $p < .05$, using GRF theory as implemented in FSL's *cluster*.

2.2.5. Multivariate pattern analysis

The aim of the multivariate pattern analysis (MVPA) in the present study was to generate, for each trial, a proxy for the activation strength of task-relevant and task-irrelevant features in the brain. To train the multivariate classifier, voxel-wise and trial-wise BOLD amplitude values were required. These were estimated using general linear model with one separate regressor for every trial (Mumford et al., 2012).

For each modality, two classifiers were constructed (Fig. 3.a). One classifier was trained for the task-relevant feature (visual: houses versus faces; somatosensory: intermittent versus continuous); the other classifier was trained for the irrelevant feature (left versus right). To select voxels containing useful activity patterns for the classifier analyses (feature selection), regions-of-interest were defined by a conjunction or disjunction of anatomical structures, as well as those voxel that were found to be active in response to specific task conditions. The regions of interest were defined for each of the classifiers in the following manner. For the somatosensory task-irrelevant region of interest, a higher-level analysis was performed using FLAME to generate statistical contrast maps of left versus right, and right versus left stimulus side. Cortical regions with threshold $z > 2$ were set to a binary value of 1, otherwise

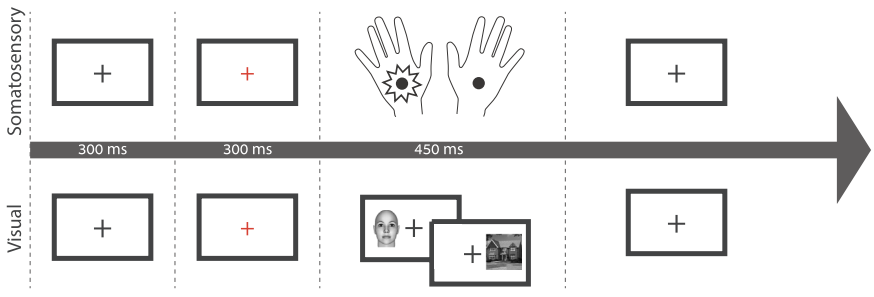

Fig. 2. Timeline of somatosensory (top) and visual (bottom) Simon task trials.

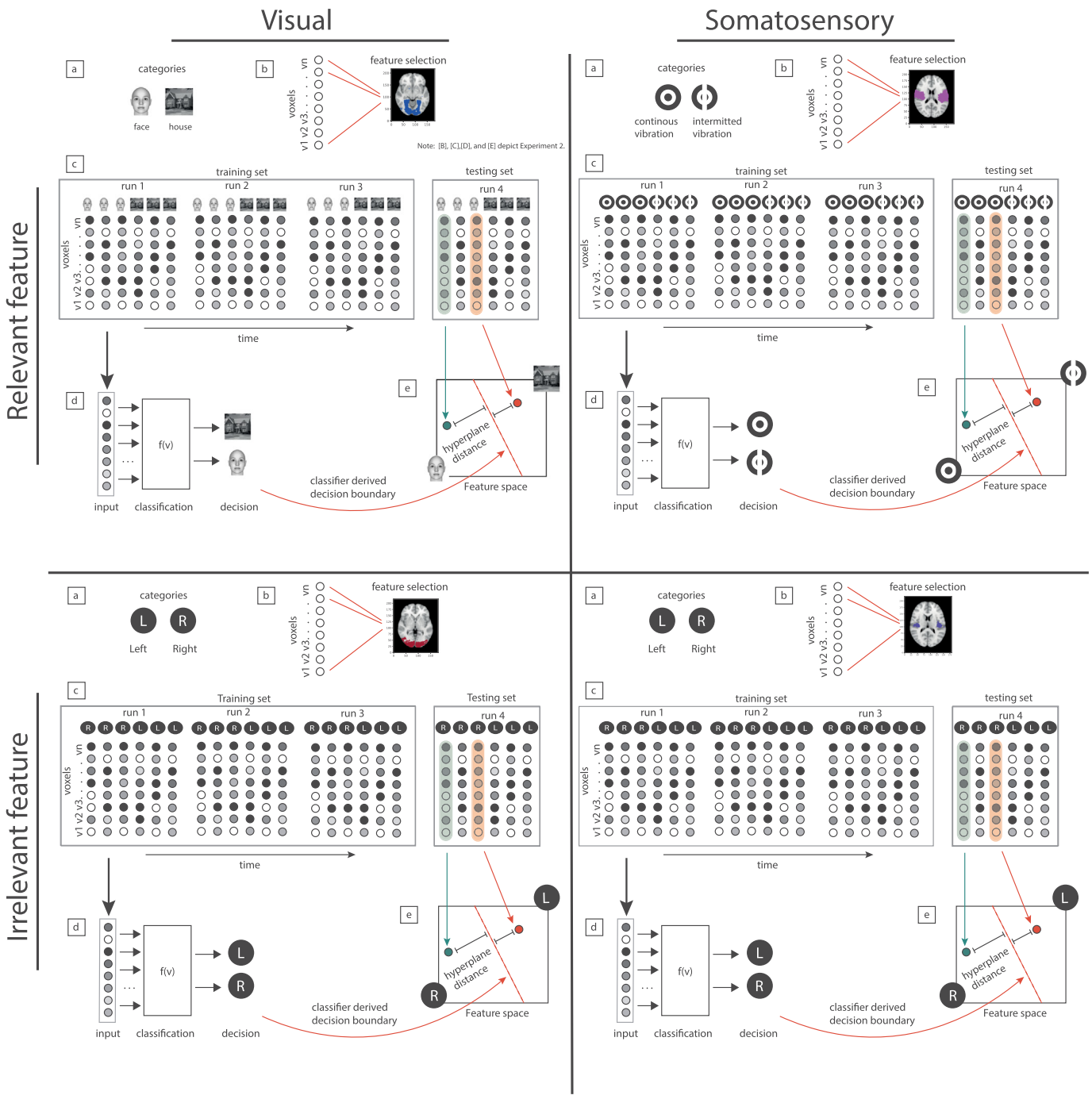

Fig. 3. Multivariate pattern analysis (MVPA) of visual (left) and somatosensory (right) datasets. For each dataset, two classifiers were trained to predict the task-relevant (top) and task-irrelevant (bottom) features, in the following manner: [a] classifier's categories were defined, and [b] region of interest was outlined. The SVM classifier [d] was trained on one subset of trials [c], i.e., training set. An n-dimensional decision boundary was defined [e]. Then the SVM classifier was tested on the other subset of trials, i.e., the testing set. Finally, the distance from the boundary [e], i.e., hyperplane distance, served as a proxy for the quality of the feature representation in the predefined region of interest.

0. Left versus right and right versus left stimulus side contrasts were summed, and then multiplied with a binary anatomical mask of the primary and secondary somatosensory cortices. Only voxels shared by the sum of the contrasts and the anatomical mask were left in for the somatosensory task-irrelevant region of interest. This was done to ensure that the search pattern of voxel activity associated with the presentation of spatial information was not contaminated with activity associated with the motor cortex. The somatosensory task-relevant region of interest was constrained by anatomical masks of the primary and secondary somatosensory cortex (Jülich Histological Atlas, Eickhoff et al., 2005, Fig. 3.b) which were then transformed to the individual functional space of each participant.

A Higher-level analysis using FLAME was applied to generate statistical contrast maps of house versus face, and face versus house conditions. Cortical regions with threshold of $z > 2$ were set a binary value of 1, otherwise 0. The binary anatomical mask of V1 to V5 was subtracted from the house versus face contrast, leaving out voxels associated with early-visual processing, but leaving in voxels associated with object representation in the ventral temporal cortex. The house versus face, and face versus house contrast masks were summed to

create the region of interest of the visual task-relevant classifier. For the task-irrelevant feature, namely stimulus side (left or right), the data set was separated into two data-sets: house trials and face trials. House task-irrelevant classifiers (i.e., trained to detect whether a house appeared on the left vs. right side of the screen), and face task-irrelevant classifiers (i.e., trained to detect whether a face appeared on the left vs. right side of the screen) were trained and tested independently on the respective data set. The region of interest for house trials was defined by the house versus face mask, and region of interest for the face trials was defined by the face versus house mask. This approach allowed to explore the pattern of activity associated with spatial representation (left or right) within the region of voxels that demonstrated high activation in response to the stimulus type (house or face) in question.

To avoid circular analysis (Kriegeskorte et al., 2009), each of the high-level contrasts needed for the masks, was generated 28 times, once for each participant. Each time, a contrast map of one participant was excluded from the group analysis (i.e., leave-one-out by participant). This way, each participant had its own individual mask, which was constructed from the group's brain activity that did not include its own. Once the masks were completed they were transformed back to the individual's functional space.

For each participant and modality, a support vector machine (SVM) (Bishop, 2006) classifier was trained on three of the four runs (Fig. 3.c, d). The fourth run was used to test how well the classifier could predict held-out data (i.e., leave-one-out by runs). For each participant, this process was repeated 16 times: for each modality dataset (visual, somatosensory), for each of the four runs, and for each of the classes of classifiers (task-relevant, task-irrelevant). This way, for each trial, in each modality, two binary scores were collected, indicating whether or not the classifiers were successful in predicting the location and the identity of the stimulus presented in the trial.

Finally, for each trial, two continuous values were collected: how far the pattern of activity on the trial was from the task-relevant classifier's n-dimensional decision boundary (i.e., hyperplane distance), and how far the pattern of activity of the trial was from the task-irrelevant boundary (Fig. 3.e). The hyperplane distance was positive for trials that were identified as left/houses/continuous, and negative for trials identified as right/faces/intermittent. For the statistical analyses, the hyperplane distances were pooled together, after changing the sign of the hyperplane distance towards the left/houses/continuous such that positive values correspond to correct identification and negative values to incorrect identification. These hyperplane values served as a proxy for the quality of the representation of these features in sensory brain areas. A larger distance is associated with a strong representation of the feature in the brain (Raizada et al., 2010). A smaller (or negative) distance is associated with a weak feature representation. Finally, repeated measures analysis of variance (ANOVA) and Bayesian ANOVA (Morey et al., 2015; Rouder et al., 2012) were computed for hyperplane distances with correctness of response and congruency as factors, to test the following predictions (Fig. 1.b): (A) the hyperplane distance of task-relevant feature is larger in correct than incorrect trials, in both congruent and incongruent trials; (B) Hyperplane distance of the task-irrelevant feature is larger in correct than incorrect congruent trials; And, (C) the hyperplane distance of the task-irrelevant feature is smaller in correct than incorrect incongruent trials.

3. Results

3.1. Behavioural Analysis

The analyses of variance focused on the main effects of congruency on accuracy and response time (Fig. 4). None of the dependent variables systematically depended on the trial length, therefore it was not included in the main analyses. In the visual task, only four participants made no errors in the congruent condition, and only one participant made no errors in the incongruent condition. In the somatosensory task,

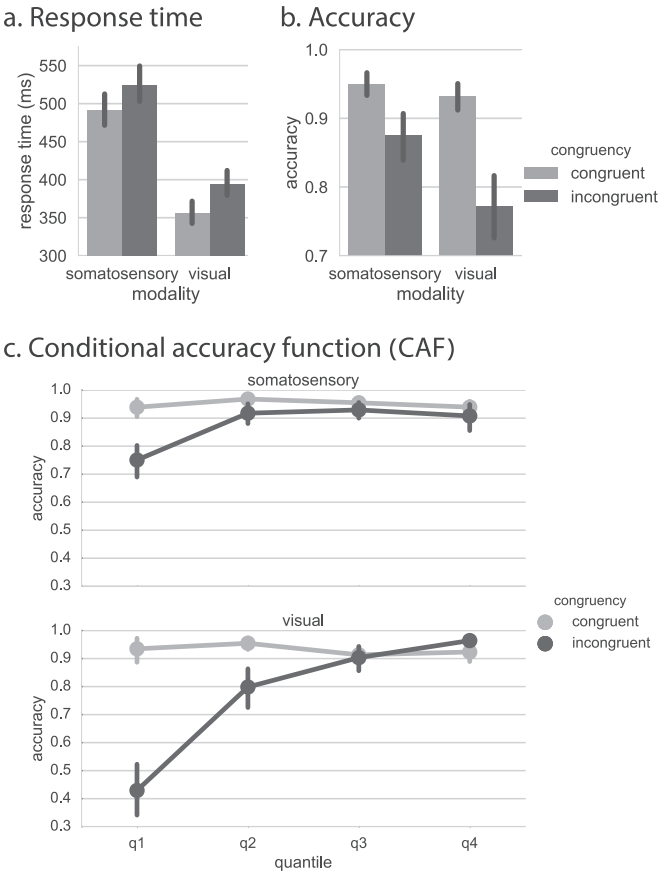

Fig. 4. Behavioural results. [a] Mean response time, [b] accuracy, and [c] conditional accuracy function (CAF), as a function of modality and congruency. Error bars denote confidence interval of 95%.

only two participants made no errors in the congruent condition. The difference in accuracy of congruent and incongruent conditions was significant in the somatosensory Simon task (congruent $M = 95\%$, $SD = 4.7\%$, incongruent $M = 87.6\%$, $SD = 9.6\%$), [$F(1, 27) = 20.41$, $MSE = 0.003$, $p = 0.000111$, and $BF_{10} = 453$], as well as in the visual Simon task (congruent $M = 93.1\%$, $SD = 5.8\%$, incongruent $M = 77.26\%$, $SD = 12.9\%$), [$F(1, 27) = 39.32$, $MSE = 0.009$, $p = 0.000001$, $BF_{10} = 596726$]. Main effects were found for response time in the somatosensory Simon task [$F(1, 27) = 66.55$, $MSE = 240$, $p = 9 \times 10^{-9}$, $BF_{10} = 572873$], as well as in the visual Simon task [$F(1, 27) = 52.77$, $MSE = 377$, $p = 8 \times 10^{-8}$, $BF_{10} = 88364$], suggesting that the responses in the congruent condition were significantly faster than responses in the incongruent condition (somatosensory: congruent $M = 490$ ms, $SD = 58$ ms; incongruent $M = 524$ ms, $SD = 61$ ms; visual: congruent $M = 356$ ms, $SD = 39$ ms; incongruent $M = 394$ ms, $SD = 54$ ms).

Conditional Accuracy Functions (CAF) were calculated for each participant, task, and congruency condition. RTs were partitioned into four quantiles or proportional bins (Fig. 4.c). Mean accuracy was calculated for each quantile. Two-way ANOVA was conducted for congruency and quantile. A significant two-way interaction was found in the visual task [$F(3, 81) = 61.51$, $MSE = 0.013$, $p < 2 \times 10^{-16}$, and $BF_{10} > 10^{+6}$]. Simple planned-comparison suggest a significant difference of 0.51 in mean accuracy between congruent and incongruent conditions in the first quantile [$F(1, 27) = 76.76$, $MSE = 0.047$, $p = 2.2 \times 10^{-9}$, and $BF_{10} > 10^{+6}$], and a significant difference of 0.16 in mean accuracy in the second quantile [$F(1, 27) = 16.7$, $MSE = 0.02$, $p = .000352$, and $BF_{10} > 10^{+6}$]. In the somatosensory task, the two-way interaction was significant [$F(3, 81) = 17.18$, $MSE = 0.004$, $p = 1.01 \times 10^{-8}$, and $BF_{10} = 529116$]. Simple planned-comparison suggest a significant difference of 0.18 in mean accuracy between

Table 1
Anatomical location and MNI coordinates for the whole-brain contrasts.

			Left Hemisphere		Right Hemisphere	
Modality	Contrast	Anatomical Area	MNI coordinates	Z max	MNI coordinates	Z max
Somatosensory	Congruent versus Incongruent		–		–	
	Incongruent vs. Congruent		–		–	
	Left vs. Right.	Secondary somatosensory cortex	–		41 −21 18	4.52
	Right vs. Left	Secondary somatosensory cortex	−40 −21 14	3.84	–	
	Continuous vs. Intermittent		–		–	
	Intermittent vs. Continuous		–		–	
Visual	Congruent vs. Incongruent		–		–	
	Incongruent vs. Congruent		–		–	
	Left vs. Right.	Visual cortex V2	–		14 −88 −10	6.9
	Right vs. Left	Visual cortex V2	−12 −91 −14	7.37		
	House vs. Face	Temporal occipital fusiform	–		25 −47 −14	6.88
	Face vs. House		–		–	

Anatomical location and MNI coordinates with z > 3.1 (p < 0.05, cluster-corrected) for the whole-brain contrast incongruent versus (vs.) congruent and left versus right, and vice versa.

congruent and incongruent conditions in the first quantile [$F(1, 27) = 31.05$, $MSE = 0.016$, $p = 6.57 \times 10^{-6}$, and $BF_{10} = 743532$] and a significant difference of 0.05 in mean accuracy between congruent and incongruent conditions in the second quantile [$F(1, 27) = 7.19$, $MSE = 0.004$, $p = 0.0123$, and $BF_{10} = 745696$].

3.2. Neuroimaging data

3.2.1. Univariate analysis

For comparison of task conditions—congruency, stimulus type, and stimulus side—high-level contrasts were produced with all 28 participants. Cortical regions with a threshold of z > 3.1 and a cluster probability of p < 0.05, corrected for whole-brain multiple comparisons (using GRF theory), are reported in Table 1. The contrast of incongruent versus congruent trials yielded no significant clusters, neither in the visual, nor in the somatosensory modality (for similar results see Forstmann et al., 2008a, 2008b; Strack et al., 2013, however, see Liu et al., 2004 and Peterson et al., 2002 for significant findings).

3.2.2. Multivariate pattern analysis

Mean accuracy scores of the visual task-relevant SVM classifier (0.59) was significantly different from chance [($t(27) = 11.11$, $p = 1.4 \times 10^{-11}$, $BF_{10} > 10^{+6}$)]. Mean accuracy scores for visual house task-irrelevant classifier (0.59) and face task-irrelevant classifier (0.53) were significantly different from chance [$t(27) = 8.51$, $p = 3.9 \times 10^{-9}$, $BF_{10} > 10^6$ and $t(27) = 2.78$, $p = 0.0097$, $BF_{10} = 4.71$, respectively]. Mean accuracy score of the somatosensory task-irrelevant classifier (0.52) and somatosensory task-relevant classifier (0.54) were significantly different from chance [$t(27) = 3.13$, $p = 0.00414$, $BF_{10} = 9.77$, and $t(27) = 4.44$, $p = 0.000135$, $BF_{10} = 200$, respectively].

Bayesian ANOVA was applied for hyperplane distances, relevant and irrelevant, in the visual and somatosensory modalities as a function of congruency (congruent, incongruent) and correctness of response (correct, incorrect) as fixed effects, and participants as random effects. None of the dependent variables systematically depended on the trial length, therefore it was not included in the main analyses. Table 2 provides detailed statistics. In what follows we will focus on the specific predictions introduced before.

3.2.2.1. Relevant feature representation. In line with the first prediction, a main effect for correctness of a trial was found in the somatosensory dataset, and a subset of the visual dataset, namely for the house stimuli but not for the face stimuli of the visual dataset. Concretely, the hyperplane distance of the relevant feature was larger for trials in which correct responses were given, as compared to those in which incorrect responses were given, as seen in Fig. 5 (somatosensory: correct $M = 0.034$, $SD = 0.043$, incorrect $M = -0.029$, $SD = 0.158$; visual-house: correct $M = 0.09$, $SD = 0.09$, incorrect $M = 0.019$, $SD = 0.19$; visual-face: correct $M = 0.06$, $SD = 0.1$, incorrect $M = 0.039$, $SD = 0.158$). The evidence acquired by the face subset of the visual dataset was inconclusive, suggesting more data needs to be collected to verify or falsify our theory. Main effects for congruency, and the interactions between congruency and correctness, were not significant in either of the modalities (see Table 2).

3.2.2.2. Irrelevant feature representation. In line with the second prediction, the two-way interaction between congruency and correctness in the somatosensory dataset was significant, with evidence strongly in favor of the interaction model (Table 2). Concretely, the hyperplane distance of the irrelevant feature in the correct incongruent condition ($M = -0.001$, $SD = 0.042$) was smaller than the hyperplane distance in the incorrect incongruent condition ($M = 0.078$, $SD = 0.146$). As expected from the third prediction, the hyperplane distance for the irrelevant feature for the correct congruent condition ($M = 0.038$, $SD = 0.047$) was larger than the hyperplane distance for the incorrect congruent condition ($M = -0.038$, $SD = 0.203$), as seen in Fig. 5. No interaction or main effects were found in either of the subsets of the visual dataset. The data acquired in the visual dataset provide inconclusive evidence for both of the hypotheses, suggesting more data needs to be collected to verify or falsify our theory. To summarize, findings in the somatosensory dataset, and to some extent in the visual dataset, support the view that sensory areas code for response capture.

4. Discussion

The neural processes that underlie encoding and resolution of conflicting information in the human brain remain elusive. While most studies describe the neural correlates of controlled inhibition (Duncan, 2001; Ridderinkhof et al., 2004; Stocco et al., 2017) and decision processes (Gold and Shadlen, 2007; Mulder et al., 2014), the present study focused on the early phase of sensory information encoding. This study presents an exciting modus operandi to answer the issue at hand: what are the neural origins and dynamics of cognitive conflict? A large body of research studying various conflict tasks has characterized fast errors as resulting from early response capture of irrelevant information (Coleman et al., 2017; Dittrich and Stahl, 2017; Duprez et al., 2016; Ellinghaus and Miller, 2017; Houvenaghel et al., 2016; Hughes and Yeung, 2011; Salzer et al., 2014; Stins et al., 2007; Wylie et al., 2009). Using a multivariate analysis techniques capitalizing on trial-to-trial variability in neural signal, we demonstrate that traces of the conflict arise in sensory brain areas that code for relevant and irrelevant

Table 2
(Bayesian) ANOVA for hyperplane distance of task-relevant and task-irrelevant features as function of correctness and congruency.

				F	df	MSE	p	BF_{10}
Somatosensory	Irrelevant	Congruency		2.46	26	0.016	0.128	0.57
		Correctness		0.04	26	0.013	0.841	0.19
		Congruency*Correctness		9.99	25	0.017	0.004*	36
	Relevant	Congruency		0.590	26	0.009	0.449	0.25
		Correctness		7.179	26	0.015	0.012*	20
		Congruency*Correctness		0.745	25	0.008	0.396	0.35
			House/Face trials	F	df	MSE	p	BF_{10}
Visual	Irrelevant	Congruency	face	0.325	26	0.028	0.574	0.21
			house	0.006	26	0.033	0.938	0.19
		Correctness	face	0.025	26	0.018	0.877	0.2
			house	0.924	26	0.012	0.345	0.25
		Congruency*Correctness	face	1.271	23	0.017	0.271	0.45
			house	0.023	22	0.018	0.881	0.28
	Relevant	Congruency	face	1.454	26	0.007	0.239	0.24
			house	0.003	26	0.018	0.955	0.2
		Correctness	face	2.108	26	0.01	0.159	0.48
			house	7.6	26	0.018	0.01*	5.48
		Congruency*Correctness	face	0.33	23	0.013	0.57	0.299
			house	0.085	22	0.03	0.774	0.34

It should be noted that errors in the congruent conditions are rare; some of the participants made no errors. This is expressed in the degrees of freedom (df), and in the relatively large variance for the congruent condition measurements, as visualized in Fig. 5.

stimulus features.

Within the framework of the dual-route model, we formulated concrete predictions in a theoretically principled way (de Hollander et al., 2016; Forstmann et al., 2016, 2011; Turner et al., 2016). We framed a qualitative association between the route's activity and the clarity of representations for stimulus features in sensory brain areas. We expected to find traces of the dynamics of the conflict in sensory brain areas that code for both relevant and irrelevant stimulus features. We operationalized the clarity of stimulus feature representation on individual trials as the distance to the hyperplane set up by the SVM classifier (Kriegeskorte and Kievit, 2013), and related the observed activity pattern to behavioural responses (Raizada and Kriegeskorte, 2010). We reasoned that to trace the neural correlates of early response capture in a MVPA fast event-related experimental design fast responses should be induced by enforcing a response deadline, and the signal-to-noise ratio should be large enough to amplify the discrepancy of the neural measures, making it possible for the classifiers to capture the appropriate data features (Bishop, 2006; Mumford et al., 2012). These principles were successfully incorporated and our predictions were corroborated. On trials in which participants made incorrect responses, the clarity of representation was generally stronger for irrelevant incompatible stimulus features, while clarity of irrelevant compatible feature representation was weaker. At the same time, on trials in which participants made correct responses, the clarity of the relevant feature representation was stronger. To summarize, understanding the mechanistic role of clarity of feature representation in sensory brain areas is demonstrated to advance our understanding of the neural origins of cognitive conflicts, and the dynamics of early response capture.

4.1. Future directions and modelling of conflict tasks

In the present study we demonstrated a qualitative linking, namely, we used the framework of the dual route model to make predictions about the differences in feature representation in sensory brain areas. Tighter links can be made using formal mathematical cognitive models, which may provide explicit and precise assumptions. A commendable candidate model is the diffusion model for conflict tasks (DMC; Ulrich et al., 2015). The DMC is a sequential sampling model whose basic assumptions derive from the dual-route model. The DMC provides a mechanistic description of an automatic accumulator of evidence driven by an irrelevant stimulus dimension on the one hand, and a deliberate accumulator of evidence for a relevant dimension on the other. Evidence from both routes is superimposed (combined) onto a single accumulating process until one of the predetermined thresholds is reached, after which a response is made. The DMC is a cognitive model explicitly designed for conflict tasks, which in contrast to other models can easily explain some benchmark findings in the Simon task, and thus constitutes a more plausible theoretical framework (Servant et al., 2016; Ulrich et al., 2015). Within the framework of the present study, it would have been tempting to correlate the model parameters with the variability as a proxy of neural feature representations. However, to the best of our knowledge, the parameters of the DMC have not been shown to be identifiable (Bamber and van Santen, 2000) and there are good reasons to think they might not be (Miletić et al., 2017; White et al., 2018). Model-based cognitive neuroscience approaches hinge on the possibility of quantifying subject-to-subject or trial-to-trial variability in cognition, so identifiability of the parameters would be highly desirable (Forstmann and Wagenmakers, 2015; Palestro et al., 2018). Other sequential sampling frameworks, as the Linear Ballistic Accumulator (Brown and Heathcote, 2008) and the Diffusion Decision Model (Ratcliff et al., 2016) therefore might be more suitable to be used with the Simon task in a model-based framework (de Hollander et al., 2016; Turner et al., 2015). However these classical sequential sampling models cannot easily explain standard findings in the Simon task (Servant et al., 2015; Ulrich et al., 2015). Clearly, the development of novel sequential sampling models that are both tractable and can explain behavioural patterns found in conflict tasks, most pressingly the Simon task, would be highly advantageous.

Crucially, we believe that all of these models come to the same prediction as the original qualitative dual-route model. At the same time, the confirmatory nature of the MVPA predictions put forward in this paper preclude any strong conclusions about other qualitative models of the Simon effect. Future work should reveal whether such models make different or comparable predictions, and whether these can be used to disambiguate between theoretical accounts of the Simon effect. Whether the variability in response activations are due to random bottom-up trial-to-trial noise (Hommel et al., 2004) or are influenced by feedback processes downstream (Ridderinkhof, 2002b), remains for now an open question. In future work, brain stimulation techniques could be used to alter activity in frontal regions (e.g., van Campen et al., 2018) to see if they influence representations in visual cortex. Also, dynamic causal modelling or laminar-resolved 7T fMRI (Stephan et al., 2017; Trampel et al., 2017) could be used to probe how much the representations in sensory areas are influenced by top-down

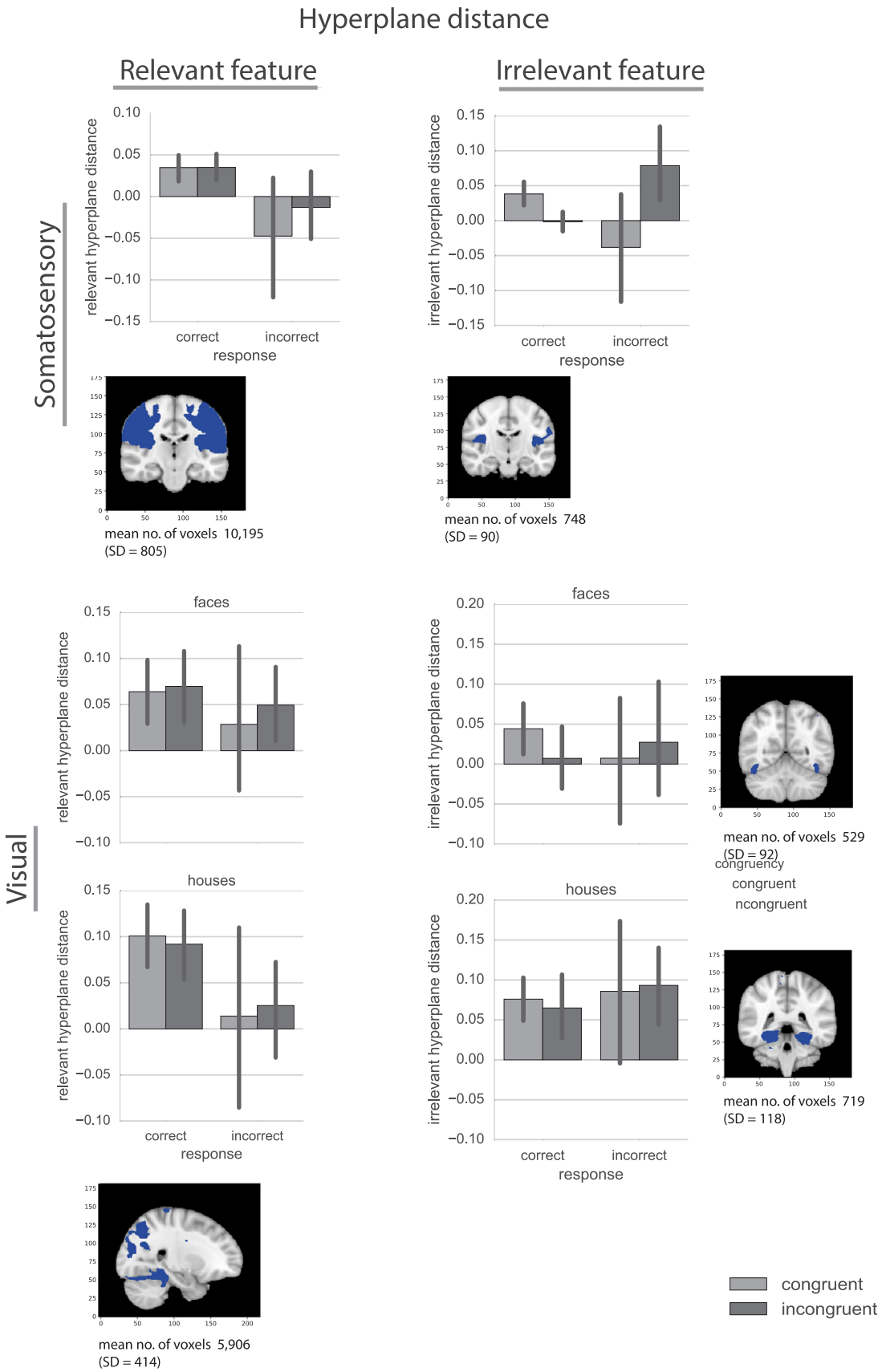

Fig. 5. Mean hyperplane distances of relevant (left) and irrelevant (right) features, in the somatosensory (top) and visual (bottom) Simon tasks, as a function of congruency and correctness of response. Brain image illustrates a representative slice of the associated region of interest. Error bars denote confidence interval of 95%. Note that a single classifier was trained for the task-relevant visual dimension (house/face), however, for an orderly graphical comparison with the irrelevant feature display, the visual data-set was split by trial type. Masks' size, i.e., mean number of voxels, and standard deviation (SD) over subjects, are reported for each mask.

signals.

The approach taken in the current study allowed us to derive specific predictions that are theoretically grounded in the dual-route model and that can be tested in the data. Using a multivariate analysis techniques we demonstrated that traces of the conflict arise in sensory brain areas that code stimulus features. Importantly, the main contribution of this study is showing that it is possible to tap into stimulus representations during the Simon task and that these representations are related to behaviour. Additional conceptual replication and implementation with other conflict tasks are necessary in order to further substantiate the hypotheses brought forth in the present study, and would advance our understanding how the brain codes and resolves conflicting information.

Acknowledgment

We would like to thank Olympia Colizoli and Anja Pahor for generating and sharing the house and face figures used in the study.

Author contributions

Y.S., G.H., L.M., and B.U.F., conceptualized the presented idea and formulated the methodology. Y.S carried out the investigation and curated the data. Y.S. and G.H. developed the formal analysis, visualization and software. Y.S. took the lead in writing of the original draft. All authors provided critical feedback, reviewing and editing the manuscript at all stages. Y.S. and B.U.F. acquired the funding. B.U.F. supervised the project.

Conflict of interest

The authors declare no competing financial interests

Funding

This work was supported by the European Research Council (ERC), European Union, grant ID Speed 313481 (to B.U.F.); by the Nederlandse Organisatie voor Wetenschappelijk Onderzoek (NWO), the Netherlands, grant ID Vidi 452-11-008 (to B.U.F.); and by the Israel Science Foundation, Israel, grant ID 93/15 (to Y.S.).

Appendix A. Supporting information

Supplementary data associated with this article can be found in the online version at doi:10.1016/j.neuropsychologia.2018.12.009.

References

Bamber, D., van Santen, J.P.H., 2000. How to assess a model's testability and identifiability. J. Math. Psychol. 44, 20–40. https://doi.org/10.1006/jmps.1999.1275.

Bishop, C.M., 2006. Pattern Recognition and Machine Learning. Springer.

Brown, S.D., Heathcote, A., 2008. The simplest complete model of choice response time: linear ballistic accumulation. Cogn. Psychol. 57, 153–178. https://doi.org/10.1016/j.cogpsych.2007.12.002.

Coleman, J.R., Watson, J.M., Strayer, D.L., 2017. Working memory capacity and task goals modulate error-related ERPs. Psychophysiology. https://doi.org/10.1111/psyp.12805.

de Hollander, G., Forstmann, B.U., Brown, S.D., 2016. Different ways of linking behavioral and neural data via computational cognitive models. Biol. Psychiatry Cogn. Neurosci. Neuroimaging 1, 101–109. https://doi.org/10.1016/j.bpsc.2015.11.004.

De Jong, R., Liang, C.C., Lauber, E., 1994. Conditional and unconditional automaticity: a dual-process model of effects of spatial stimulus-response correspondence. J. Exp. Psychol. Hum. Percept. Perform. 20, 731–750.

Dittrich, K., Stahl, C., 2017. Two distinct patterns of interference in between-attribute Stroop matching tasks. Atten. Percept. Psychophys. 79, 563–581.

Duncan, J., 2001. An adaptive coding model of neural function in prefrontal cortex. Nat. Rev. Neurosci. 2, 820–829. https://doi.org/10.1038/35097575.

Duprez, J., Houvenaghel, J.F., Naudet, F., Dondaine, T., Auffret, M., Robert, G., Drapier, D., Argaud, S., Vérin, M., Sauleau, P., 2016. Evaluating cognitive action control using eye-movement analysis: an oculomotor adaptation of the Simon task. Front. Hum. Neurosci. 10, 1–8. https://doi.org/10.3389/fnhum.2016.00084.

Eickhoff, S.B., Stephan, K.E., Mohlberg, H., Grefkes, C., Fink, G.R., Amunts, K., Zilles, K., 2005. A new SPM toolbox for combining probabilistic cytoarchitectonic maps and functional imaging data. Neuroimage 25, 1325–1335. https://doi.org/10.1016/j.neuroimage.2004.12.034.

Ellinghaus, R., Miller, J., 2017. Delta plots with negative-going slopes as a potential marker of decreasing response activation in masked semantic priming. Psychol. Res. https://doi.org/10.1007/s00426-017-0844-z. (0, 0).

Forstmann, B.U., Jahfari, S., Scholte, S.H., Wolfensteller, U., van den Wildenberg, W.P.M., Ridderinkhof, R.K., 2008a. Function and structure of the right inferior frontal cortex predict individual differences in response inhibition: a model-based approach. J. Neurosci. 28, 9790–9796. https://doi.org/10.1523/JNEUROSCI.1465-08.2008.

Forstmann, B.U., Ratcliff, R., Wagenmakers, E.J., 2016. Sequential sampling models in cognitive neuroscience: advantages, applications, and extensions. Annu. Rev. Psychol. 67, 641–666. https://doi.org/10.1146/annurev-psych-122414-033645.

Forstmann, B.U., van den Wildenberg, W.P.M., Ridderinkhof, R.K., 2008b. Neural mechanisms, temporal dynamics, and individual differences in interference control. J. Cogn. Neurosci. 20, 1854–1865. https://doi.org/10.1162/jocn.2008.20122.

Forstmann, B.U., Wagenmakers, E.J., 2015. An Introduction to Model-based Cognitive Neuroscience. Springerhttps://doi.org/10.1017/CBO9781107415324.004.

Forstmann, B.U., Wagenmakers, E.J., Eichele, T., Brown, S., Serences, J.T., 2011. Reciprocal relations between cognitive neuroscience and formal cognitive models: opposites attract? Trends Cogn. Sci. 15, 272–279. https://doi.org/10.1016/j.tics.2011.04.002.

Gold, J., Shadlen, M., 2007. The neural basis of decision making. Annu. Rev. Neurosci. 30, 535–574. https://doi.org/10.1146/annurev.neuro.29.051605.113038.

Gorgolewski, K., Burns, C.D., Madison, C., Clark, D., Halchenko, Y.O., Waskom, M.L., Ghosh, S.S., 2011. Nipype: a flexible, lightweight and extensible neuroimaging data processing framework in python. Front. Neuroinform. 5, 13. https://doi.org/10.3389/fninf.2011.00013.

Haxby, J.V., Connolly, A.C., Guntupalli, J.S., 2014. Decoding neural representational spaces using multivariate pattern analysis. Annu. Rev. Neurosci. 435–456. https://doi.org/10.1146/annurev-neuro-062012-170325.

Hommel, B., Proctor, R.W., Vu, K.P.L., 2004. A feature-integration account of sequential effects in the Simon task. Psychol. Res. 68, 1–17. https://doi.org/10.1007/s00426-003-0132-y.

Houvenaghel, J.F., Duprez, J., Argaud, S., Naudet, F., Dondaine, T., Robert, G.H., Drapier, S., Haegelen, C., Jannin, P., Drapier, D., Verin, M., Sauleau, P., 2016. Influence of subthalamic deep-brain stimulation on cognitive action control in incentive context. Neuropsychologia 91, 519–530. https://doi.org/10.1016/j.neuropsychologia.2016.09.015.

Hughes, G., Yeung, N., 2011. Dissociable correlates of response conflict and error awareness in error-related brain activity. Neuropsychologia 49, 405–415. https://doi.org/10.1016/j.neuropsychologia.2010.11.036.

Jenkinson, M., 2004. Improving the registration of B0-disorted EPI images using calculated cost function weights. Neuroimage 22, e1544–145.

Jezzard, P., Balaban, R.S., 1995. Correction for geometric distortion in echo planar images from B0 field variations. Magn. Reson. Med. 34, 65–73.

Kornblum, S., Hasbroucq, T., Osman, A., 1990. Dimensional overlap: cognitive basis for stimulus-response compatibility-A model and taxonomy. Psychol. Rev. 97, 253–270.

Kriegeskorte, N., 2011. Pattern-information analysis: from stimulus decoding to computational-model testing. Neuroimage 56, 411–421. https://doi.org/10.1016/j.neuroimage.2011.01.061.

Kriegeskorte, N., Kievit, R.A., 2013. Representational geometry: integrating cognition, computation, and the brain. Trends Cogn. Sci. 17, 401–412. https://doi.org/10.1016/j.tics.2013.06.007.

Kriegeskorte, N., Simmons, W.K., Bellgowan, P.S.F., Baker, C.I., 2009. Circular analysis in systems neuroscience: the dangers of double dipping. Nat. Neurosci. 12, 535–540. https://doi.org/10.1167/8.6.88.

Liu, X., Banich, M.T., Jacobson, B.L., Tanabe, J.L., 2004. Common and distinct neural substrates of attentional control in an integrated Simon and spatial Stroop task as assessed by event-related fMRI. Neuroimage 22, 1097–1106. https://doi.org/10.1016/j.neuroimage.2004.02.033.

Miletić, S., Turner, B.M., Forstmann, B.U., van Maanen, L., 2017. Parameter recovery for the Leaky Competing Accumulator model. J. Math. Psychol. 76, 25–50. https://doi.org/10.1016/j.jmp.2016.12.001.

Morey, R.D., Rouder, J.N., Jamil, T., 2015. Package BayesFactor.

Mulder, M.J., van Maanen, L., Forstmann, B.U., 2014. Perceptual decision neurosciences - a model-based review. Neuroscience 277, 872–884. https://doi.org/10.1016/j.neuroscience.2014.07.031.

Mumford, J.A., Turner, B.O., Ashby, F.G., Poldrack, R.A., 2012. Deconvolving BOLD activation in event-related designs for multivoxel pattern classification analyses. Neuroimage 59, 2636–2643. https://doi.org/10.1016/j.neuroimage.2011.08.076.

Palestro, J.J., Sederberg, P.B., Osth, A.F., Van Zandt, T., Turner, B.M., 2018. Likelihood-Free Methods for Cognitive Science.

Peterson, B.S., Kane, M.J., Alexander, G.M., Lacadie, C., Skudlarski, P., Leung, H.C., May, J., Gore, J.C., 2002. An event-related functional MRI study comparing interference effects in the Simon and Stroop tasks. Brain Res. Cogn. Brain Res. 13, 427–440.

Raizada, R.D.S., Kriegeskorte, N., 2010. Pattern-information fMRI: new questions which it opens up and challenges which face it. Int. J. Imaging Syst. Technol. 20, 31–41. https://doi.org/10.1002/ima.20225.

Raizada, R.D.S., Tsao, F.M., Liu, H.M., Kuhl, P.K., 2010. Quantifying the adequacy of neural representations for a cross-language phonetic discrimination task: prediction of individual differences. Cereb. Cortex 20, 1–12. https://doi.org/10.1093/cercor/bhp076.

Ratcliff, R., Smith, P.L., Brown, S.D., McKoon, G., 2016. Diffusion decision nodel: current issues and history. Trends Cogn. Sci. 20, 260–281. https://doi.org/10.1016/j.tics.

2016.01.007.
Ridderinkhof, K.R., 2002a. Micro- and macro-adjustments of task set: activation and suppression in conflict tasks. Psychol. Res. 66, 312–323. https://doi.org/10.1007/s00426-002-0104-7.
Ridderinkhof, K.R., 2002b. Activation and suppression in conflict tasks: empirical clarification through distributional analyses. In: Prinz, W., Hommel, B. (Eds.), Common Mechanisms in Perception and Action. Attention & Performance. Oxford University Press, Oxford, pp. 494–519.
Ridderinkhof, K.R., Ullsperger, M., Crone, E.A., Nieuwenhuis, S., 2004. The role of the medial frontal cortex in cognitive control. Science 306, 443–447. https://doi.org/10.1126/science.1100301.
Rouder, J.N., Morey, R.D., Speckman, P.L., Province, J.M., 2012. Default Bayes factors for ANOVA designs. J. Math. Psychol. 56, 356–374. https://doi.org/10.1016/j.jmp.2012.08.001.
Salzer, Y., Aisenberg, D., Oron-Gilad, T., Henik, A., 2014. In touch with the Simon effect. Exp. Psychol. 61, 165–179. https://doi.org/10.1027/1618-3169/a000236.
Salzer, Y., de Hollander, G., Forstmann, B.U., 2017. Sensory neural pathways revisited to unravel the temporal dynamics of the Simon effect: a model-based cognitive neuroscience approach. Neurosci. Biobehav. Rev. 77, 48–57. https://doi.org/10.1016/j.neubiorev.2017.02.023.
Servant, M., White, C., Montagnini, A., Burle, B., 2016. Linking theoretical decision-making mechanisms in the Simon task with electrophysiological data: a model-based neuroscience study in humans. J. Cogn. Neurosci. 28, 1501–1521. https://doi.org/10.1162/jocn.
Servant, M., White, C., Montagnini, A., Burle, B., 2015. Using covert response activation to test latent assumptions of formal decision-making models in humans. J. Neurosci. 35, 10371–10385. https://doi.org/10.1523/JNEUROSCI.0078-15.2015.
Smith, S.M., 2002. Fast robust automated brain extraction. Hum. Brain Mapp. 17, 143–155. https://doi.org/10.1002/hbm.10062.
Smith, S.M., Jenkinson, M., Woolrich, M.W., Beckmann, C.F., Behrens, T.E.J., Johansen-Berg, H., Bannister, P.R., De Luca, M., Drobnjak, I., Flitney, D.E., Niazy, R.K., Saunders, J., Vickers, J., Zhang, Y., De Stefano, N., Brady, J.M., Matthews, P.M., 2004. Advances in functional and structural MR image analysis and implementation as FSL. Neuroimage 23, 208–219. https://doi.org/10.1016/j.neuroimage.2004.07.051.
Stephan, K.E., Petzschner, F.H., Kasper, L., Bayer, J., Wellstein, K.V., Stefanics, G., Pruessmann, K.P., Heinzle, J., 2017. Laminar fMRI and computational theories of brain function. Neuroimage 1–8. https://doi.org/10.1016/j.neuroimage.2017.11.001.
Stins, J., Polderman, J., Boomsma, D., De Geus, E., 2007. Conditional accuracy in response interference tasks: evidence from the Eriksen flanker task and the spatial conflict task. Adv. Cogn. Psychol. 3, 409–417. https://doi.org/10.2478/v10053-008-0005-4.
Stocco, A., Murray, N.L., Yamasaki, B.L., Renno, T.J., Nguyen, J., Prat, C.S., 2017. Individual differences in the Simon effect are underpinned by differences in the competitive dynamics in the basal ganglia: an experimental verification and a computational model. Cognition 164, 31–45. https://doi.org/10.1016/j.cognition.2017.03.001.
Strack, G., Kaufmann, C., Kehrer, S., Brandt, S., Stürmer, B., 2013. Anticipatory regulation of action control in a Simon task: behavioral, electrophysiological, and fMRI correlates. Front. Psychol. 4, 1–14. https://doi.org/10.3389/fpsyg.2013.00047.
Stroop, J.R., 1935. Studies of interference in serial verbal reactions. J. Exp. Psychol. 18, 643–662. https://doi.org/10.1037/h0054651.
Trampel, R., Bazin, P.L., Pine, K., Weiskopf, N., 2017. In-vivo magnetic resonance imaging (MRI) of laminae in the human cortex. Neuroimage 1–9. https://doi.org/10.1016/j.neuroimage.2017.09.037.
Turner, B.M., Forstmann, B.U., Love, B.C., Palmeri, T.J., Van Maanen, L., 2016. Approaches to analysis in model-based cognitive neuroscience. J. Math. Psychol. 76, 65–79. https://doi.org/10.1016/j.jmp.2016.01.001.
Turner, B.M., van Maanen, L., Forstmann, B.U., 2015. Informing cognitive abstractions through neuroimaging: the neural drift diffusion model. Psychol. Rev. 122, 312–336. https://doi.org/10.1037/a0038894.
Ulrich, R., Schroter, H., Leuthold, H., Birngruber, T., 2015. Automatic and controlled stimulus processing in conflict tasks: superimposed diffusion processes and delta functions. Cogn. Psychol. 78, 148–174. https://doi.org/10.1016/j.cogpsych.2015.02.005.
van Campen, A.D., Kunert, R., van den Wildenberg, W.P.M., Ridderinkhof, K.R., 2018. Repetitive transcranial magnetic stimulation over inferior frontal cortex impairs the suppression (but not expression) of action impulses during action conflict. Psychophysiology 55. https://doi.org/10.1111/psyp.13003.
van Maanen, L., Turner, B., Forstmann, B.U., 2015. From model-based perceptual decision-making to spatial interference control. Curr. Opin. Behav. Sci. 1, 72–77. https://doi.org/10.1016/j.cobeha.2014.10.010.
White, C.N., Servant, M., Logan, G.D., 2018. Testing the validity of conflict drift-diffusion models for use in estimating cognitive processes: a parameter-recovery study. Psychon. Bull. Rev. 25, 286–301.
Woolrich, M.W., Jbabdi, S., Patenaude, B., Chappell, M., Makni, S., Behrens, T., Beckmann, C., Jenkinson, M., Smith, S.M., 2009. Bayesian analysis of neuroimaging data in FSL. Neuroimage 45, 173–186. https://doi.org/10.1016/j.neuroimage.2008.10.055.
Worsley, K.J., Friston, K.J., 1995. Analysis of fMRI time-series revisited—again. Neuroimage.
Wylie, S.A., van den Wildenberg, W.P.M., Ridderinkhof, K.R., Bashore, T.R., Powell, V.D., Manning, C.A., Wooten, G.F., 2009. The effect of Parkinson's disease on interference control during action selection. Neuropsychologia 47, 145–157. https://doi.org/10.1016/j.neuropsychologia.2008.08.001.